Synthetic trees for enhanced solar evaporation and water harvesting •

Cite as: Appl. Phys. Lett. **118**, 251601 (2021); doi: 10.1063/5.0049904 Submitted: 10 March 2021 · Accepted: 18 May 2021 · Published Online: 22 June 2021







Ndidi L. Eyegheleme,¹ Weiwei Shi,² Lance H. De Koninck,² Julia L. O'Brien,¹ and Jonathan B. Boreyko^{1,a)} (1)

AFFILIATIONS

- ¹Department of Mechanical Engineering, Virginia Tech, Blacksburg, Virginia 24061, USA
- ²Department of Biomedical Engineering and Mechanics, Virginia Tech, Blacksburg, Virginia 24061, USA

ABSTRACT

Solar steam generation from a porous evaporator is a promising approach for harvesting fresh water. Parasitic heat loss can be reduced by using a 3D evaporator that extends above the free surface; however, capillary rise constrains the height of such structures to a centimeter scale. Here, we demonstrate solar steam generation from a synthetic tree, which uses transpiration instead of capillary rise to pump water up insulating tubes of any desired height. A nanoporous ceramic disk coated with graphite was used for the synthetic leaf, which was attached to the upper end of a vertical array of plastic tubes. Using a solar still, it was observed that the synthetic tree harvested approximately three times more condensed water than an equivalent bulk reservoir.

Published under an exclusive license by AIP Publishing. https://doi.org/10.1063/5.0049904

Water scarcity is becoming a threat to human welfare, affecting nearly two-thirds of the global population. Solar steam generation, where water efficiently evaporates from a thermally absorptive and porous material, can be used for water harvesting when coupled with a condenser. Solar steam generators typically evaporate about 2–3 times more water compared to a bulk reservoir. Initial reports on solar steam generation utilized membranes or plasmonic nanoparticles that floated directly on the free surface, such that parasitic heat losses were still appreciable.

To further reduce these parasitic heat losses, several recent solar steam generators utilized three-dimensional porous structures extending above the free surface. $^{5,6,28-33}$ Water from the reservoir continuously wicks up a floating porous column(s) and subsequently evaporates from a thermally absorptive material. The height above the free surface where evaporation occurs tends to range from $H \approx 1$ –10 cm. This enabled a solar conversion efficiency as high as $\eta = 98\%$ compared to only $\eta = 82\%$ for a flat membrane. Efficiency is defined as $\eta = jh_{\rm lv}/q_{\rm solar}$, where $h_{\rm lv}$ is the latent heat of vaporization, j is the evaporative mass flux, and $q_{\rm solar}$ is the solar irradiation. Besides floating a tall structure directly on the free surface, an additional approach is to suspend a photothermal fabric in the air between two reservoirs. This approach resulted in an efficiency of $\eta = 90\%$, a dramatic improvement compared to $\eta = 35\%$ when floating the same fabric directly on the water.

While existing three-dimensional solar steam generators have achieved a near-perfect evaporation efficiency, several inherent

constraints limit their scope of application. One major limitation is the capillary limit; beyond a critical column height (or length of suspended fabric), the water cannot wick fast enough to replenish the evaporated water due to the increased viscous resistance. Indeed, a recent report observed a nearly threefold decrease in the evaporation rate when increasing the column height from $H=3~\rm cm$ to $4~\rm cm$ for this reason. While a height of $H\sim 1~\rm cm$ may be enough to prevent virtually all parasitic heat losses, much larger heights would be beneficial for applications involving underground water extraction. When using a seawater reservoir, another major issue is the accumulation of salt within the pores of the three-dimensional structure over time. 6,29,33,34 While accumulated salt/brine can be partially removed by having it fall/drip from the structure at a critical concentration, this is imperfect and in some cases requires active tilting.

We hypothesize that both of these constraints to current three-dimensional solar steam generators, the centimetric capillary limit and salt contamination, could be bypassed by replacing the capillary action with transpiration. In natural trees, the transpiration cycle is driven by a negative water potential generated when water evaporates from the nanoporous leaves. ^{35–41} This potential then acts across the continuous water columns within the xylem conduits, generating a hydraulic load to pump the water. Synthetic trees evaporate water from nanoporous media (i.e., "leaves") to generate a negative Laplace pressure, which can then be used to pump water across microchannels or tubes attached to the nanopores. ^{42–54} Most synthetic trees are built onto

a) Author to whom correspondence should be addressed: boreyko@vt.edu

silicon chips or only pump water up a single microcapillary tube. A very recent work proved the concept of a large-scale synthetic tree, which pumped water up a scalable array of tall, vertically oriented plastic tubes of millimetric diameter. This initial report of a large tree was limited by a slow, diffusive evaporation rate from the nanoporous leaf and also did not use a solar still to condense the water vapor emanating from the leaf. A recent perspective paper hypothetically discusses the appeal of using synthetic trees for solar steam generation, as the transpiration cycle promotes the long-range transport of water from the bulk reservoir to the evaporating interface. However, to date a transpiration-powered large-scale synthetic tree has never been used for solar steam generation and water harvesting.

Here, we show that a synthetic tree can serve as a threedimensional solar steam generator that bypasses the capillary limit entirely, by using transpiration to elevate the water to the evaporating interface. By embedding the upper ends of an array of insulating vertical tubes into a nanoporous disk, we can completely thermally decouple the evaporating interface from the bulk reservoir. Water evaporating from the nanoporous "leaf" is replenished by virtue of its negative Laplace pressure, which continuously pumps more water from a bottom reservoir up the tube array. The evaporation rate of the synthetic leaf was enhanced by spraying it with graphite and using a solar lamp. When using a solar still to collect the vapor, we found that the graphite-coated synthetic tree could evaporate and re-condense three times more water compared to a bulk reservoir under the same conditions. While fresh water was used for this preliminary study, a recent report indicates that our transpiration-based approach could also filter out salt at the intake by optionally attaching a filter.⁵

A synthetic tree was fabricated by embedding one end of a 19-tube array within a 7 mm thick nanoporous ceramic disk. The commercially available disk (Soilmoisture Equipment Corp), serving as the synthetic leaf, exhibited an average nanopore diameter of 160 nm, a porosity of $\phi=0.32$, and a cross-sectional area of $A_{\rm leaf}=22.9\,{\rm cm}^2$. Each of the 19 plastic tubes, imitating the xylem conduits, exhibited an inner diameter of $D=3.175\,{\rm mm}$ and a height of $H=6\,{\rm cm}$. Given that water ascent is powered by transpiration instead of capillary rise, it is important to note that these dimensions were arbitrary choices. We have previously shown that the tubes can be at least 3 m tall if desired. Similar to this previous report, recesses were drilled into the nanopores to embed the tubes and the seams were sealed with a water

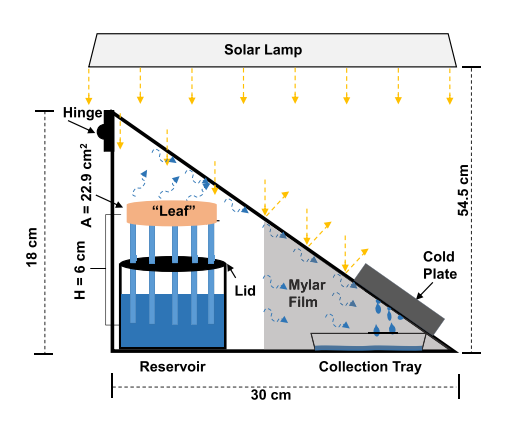
resistant epoxy. To enhance the thermal absorptivity of the synthetic leaf, for a subset of trials, the leaf was spray-coated with graphite.

A solar still was made by cutting and bonding acrylic sheets (McMaster-Carr, 8560k213). The dimensions of the solar still were a triangular cross section with a 18 cm height and a 30 cm base, with an extruded width of 16.5 cm. A rectangular hole was cut into the sloped roof of the solar still, to accommodate a $16.5 \times 4.5 \,\mathrm{cm}^2$ cold plate (McMaster-Carr, 35035K32) attached to a circulating chiller (Thermo Scientific, Accel 500 LT). In other words, we elected to use an actively cooled solar still to enhance the vapor-to-liquid conversion efficiency. The solar lamp (VIVOSUN Intertek 400588) was attached to a horizontal bar that was positioned 54.5 cm above the base of the solar still. A previous report using the same lamp estimated an irradiance of $q_{\rm solar} \approx 433 \, {\rm W/m}^2$ on an aluminum sheet placed about 30 cm beneath the lamp.⁵⁸ The side of the solar still that encompassed the cold plate was externally wrapped in Mylar film to minimize heating from the solar lamp. The reservoir of bulk water, synthetic tree (in a subset of experiments), and the collection tray (Fig. 1) were placed in the chamber using the hinged door. The seams of the door were then sealed with paraffin to minimize the leakage of water vapor building up within the solar still.

The cold plate was set to $T=15.3\pm0.4\,^{\circ}$ C, which corresponds to 1 $^{\circ}$ C beneath the dew point with respect to the ambient air outside of the chamber. This small difference between the cold plate temperature and the external dew point ensured that any appreciable condensation would be due to an internal supersaturation building up within the solar still. This was confirmed by a control experiment, where the water reservoir and synthetic tree were removed from the solar still, such that no excess water vapor was supplied to the chamber. After 3 h of testing without any water in the solar still, no appreciable condensation formed on the surface of the cold plate.

Prior to running an experimental trial, a pot of distilled water was boiled for 3 h on a 300 °C hot plate to degas the water. This pot was then sealed and left overnight to allow the water to return to room temperature. For experiments additionally utilizing a synthetic tree, the tree was constructed by embedding and sealing the top ends of 19 plastic tubes with a ceramic nanoporous disk, using a protocol identical to a previous report [Fig. 2(a) and 2(b)]. To fit within our small-scale solar still, each tube was 6 cm tall, but this could be extended to a tree height of many meters if desired. The free ends of the tube array

(a) Transpiration-Powered Synthetic Tree



(b) Photograph of setup



FIG. 1. (a) Schematic and (b) photograph of the experimental setup, where the synthetic tree was placed above a water reservoir within a solar still. Water was pumped from the reservoir to the synthetic leaf across 19 vertical plastic tubes (each with an inner diameter of 3.175 mm), by virtue of the leaf's negative Laplace pressure. The leaf was uncoated for one set of experiments and sprayed with a thermally adsorptive graphite coating for another set. A control experiment simply removed the tree but retained the bulk reservoir (the leaf and reservoir both exhibited the same 22.9 cm² area). The inset shows a close-up of the synthetic tree.

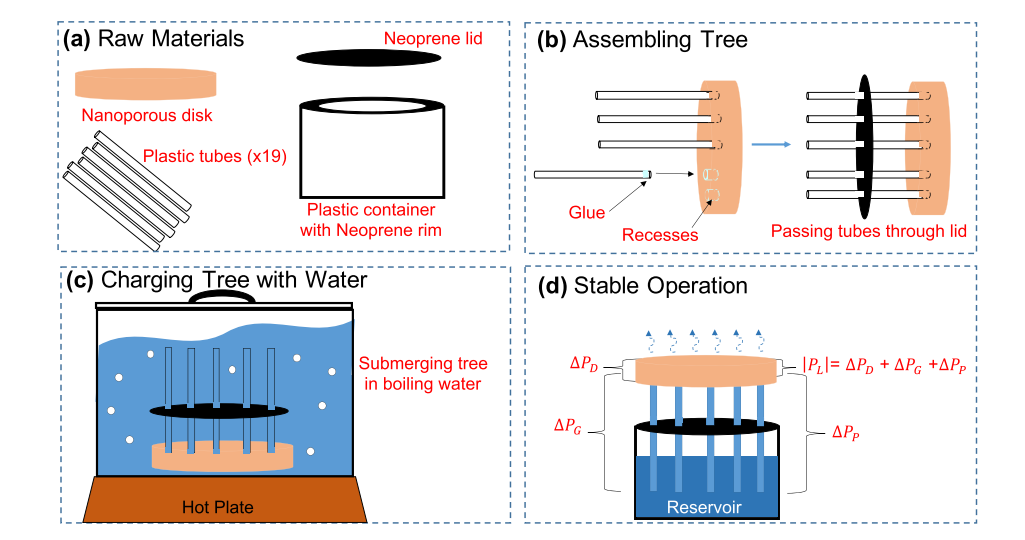


FIG. 2. Diagrams depicting the assembly of the synthetic tree. (a) The tree was composed of a nanoporous ceramic disk (leaf), an array of 19 plastic tubes (xylem conduits), and a Neoprene lid. (b) Each tube was inserted into a recess drilled into the top face of the leaf and the seam was sealed air-tight with an epoxy. (c) Prior to running an experiment in the solar still, the assembled tree was pre-filled with degassed water by submerging it in a pot of boiling water. (d) The primed tree was held above a reservoir within the solar still to demonstrate the solar steam generation and subsequent water harvesting from the condenser. The negative Laplace pressure (P_L) generated within the leaf is used to overcome the Darcy (P_D) , Poiseuille $(P_{\rm P})$, and hydrostatic $(P_{\rm G})$ pressure drops.

were passed through the snug holes of a neoprene lid, with the bottom 4.3 cm of the tube height being beneath the lid and 1.7 cm above. For the case of a thermally absorptive leaf, the top face of the nanoporous ceramic disk was uniformly sprayed with a graphite coating (Grainger Industries, 4JB39) after the tree was fabricated. Using the same pot of boiling water, the tree was fully submerged and boiled for 3 h after pre-boiling the water for 1 h [Fig. 2(c)]. This was done to ensure that the tubes and nanopores of the tree were fully charged with degassed water. As with the control reservoir, the reservoir containing the tree was allowed to cool overnight to room temperature prior to running an experiment. After cooling, a plastic reservoir was submerged into the pot of water and was held about the free ends of the tubes. The nanoporous leaf was then removed from the water and raised about 5 cm above the free surface of the plastic reservoir, such that roughly 1 cm of the 6-cm-long tubes was still submerged. The top of the lid featured a neoprene ring that supported the neoprene lid bound to the xylem conduits [Fig. 2(d)].

The solar lamp and circulating chiller were powered on 30 min prior to an experimental trial. To determine what cold plate temperature would correspond to $1\,^{\circ}\text{C}$ below the dew point of the outer

laboratory environment, the ambient temperature and relative humidity were recorded with a hygrometer. Tests were carried out for three different cases: a control case of a bulk water reservoir only, an uncoated synthetic tree extending from the same water reservoir, and finally a synthetic tree featuring the more thermally absorptive leaf. For any given setup, the water mass within the reservoir was measured before and after running a 3 h trial using a digital mass balance (OHAUS Scout, Model STX1202). Similarly, the collection tray was measured before (i.e., tare value) and after each trial to determine the amount of harvested water. The mass fluxes shown in Fig. 3 were obtained by assuming a fixed rate of evaporation/condensation throughout the duration of a 3 h trial.

Figure 3 compares the performance of the solar still under the three different experimental conditions. In Fig. 3(a), the averaged mass flux of water evaporating from within the solar still is shown. The fluxes were $j_e = 0.32 \, \mathrm{kg \ m^{-2} \ h^{-1}}$ for the uncoated tree and 0.37 kg m⁻² h⁻¹ for the black coated tree, as opposed to only $j_e = 0.14 \, \mathrm{kg \ m^{-2} \ h^{-1}}$ for the control case of bulk water. In other words, compared to bulk water, the evaporation rate was increased by a factor of 2.24 for the uncoated synthetic tree and 2.61 for the coated tree.

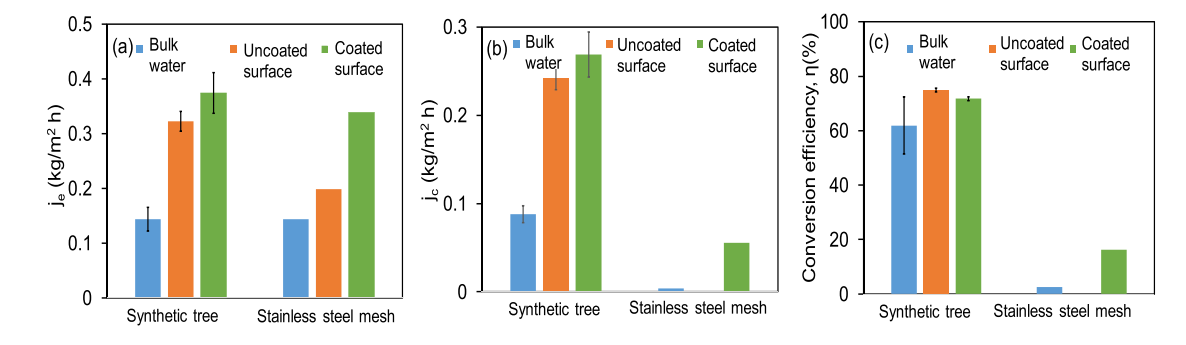


FIG. 3. Comparisons of the (a) evaporation mass flux, (b) condensation mass flux, and (c) conversion efficiency ($\eta = j_c/j_e$) for bulk water, our synthetic trees, and floating stainless steel meshes from a previous work. The mass fluxes for the stainless steel meshes were normalized by multiplying their actual values by 0.36, to account for the differing solar irradiance between setups. In this way, the evaporation flux for the bulk water control case was made equivalent across both setups. Each value for our experiment is an average of three trials and the error bars indicate one standard deviation.

Additionally, we compare our results to a previous report by Zhang et al., which used a classical solar steam generator within a solar still.3 The floating membrane from this previous report was comprised of a stainless steel mesh coated with polypyrrole (a photothermal polymer) and fluoroalkylsilane (to render hydrophobic).3 To account for the differing solar irradiance of our setup to that of Zhang et al., we multiplied the flux measurements of the latter by a factor of 0.36 such that the bulk water control case now exhibits an equivalent evaporation flux. This is consistent with the fact that Zhang et al. used 1 sun for their irradiance, whereas the irradiance of our lamp is less than half a sun. It can be seen that our uncoated synthetic tree evaporated nearly twice as much water as the uncoated stainless steel mesh, while our photothermal tree evaporated slightly more water compared to the photothermal mesh. This result confirms that using a synthetic tree for solar steam generation can result in superior evaporation rates compared to a floating photothermal membrane and also bypasses the capillary limit to allow the evaporating interface to be elevated far above the water supply.

This increase in water evaporating within the solar still when using a synthetic tree also resulted in a substantive increase in the mass flow rate of condensate harvested by the solar still [Fig. 3(b)]. Specifically, $j_c = 0.087 \, \mathrm{kg \ m^{-2} \ h^{-1}}$ for the solar still containing only bulk water vs $j_c = 0.24 \, \mathrm{kg \ m^{-2} \ h^{-1}}$ and 0.27 for the uncoated and coated trees, respectively. This corresponds to the condensation rate increasing by a factor of 2.75 for the solar still containing the uncoated tree and a factor of 3.06 for the coated tree. Our solar still harvested nearly an order of magnitude more water compared to the previously reported solar still that used a floating photothermal membrane.³ We attribute this primarily to the different heat sink used: We employed a liquid-cooled plate, whereas the previous report simply used a fan, and secondarily to the slightly enhanced evaporation rate of our tree resulting in more water vapor within the solar still.

A conversion efficiency was defined as the ratio of evaporated vapor to harvested condensate: $\eta = j_c/j_e$. The average efficiency of each setup was $\eta = 62\%$, 75%, and 72% for the bulk water, uncoated tree, and coated tree, respectively [Fig. 3(c)]. We attribute the higher conversion efficiency of the trees (compared to the bulk) to their higher evaporation rate. This can be rationalized by considering the diffusion equation governing the condensation rate on the cold plate: $j_c = D(c_{\infty} - c_{\rm p})/L$, where j_c is the mass flux of condensing water, D is the diffusivity of water vapor in air, c_{∞} is the concentration of water vapor above the evaporating interface, cp is the concentration of saturated water on the cold plate, and L is the characteristic diffusive length scale at the cold plate. The value of c_p is constant across all experiments due to the fixed temperature of the cold plate. Therefore, assuming L is also of the same order for all experiments, the only difference between the bulk water and the trees is the evaporation rate, which would influence c_{∞} within the solar still. Increasing c_{∞} increases $j_c \propto (c_{\infty} - c_{\rm p})$ by an even larger amount, which explains why the increase in evaporation rate for the trees results in a disproportionately larger increase in the resulting condensation rate. In comparison, the previously reported solar still with a photothermal membrane only had an efficiency of $\eta = 16\%$, which as already mentioned is primarily due to the differing heat sink.

The latent heat dumped into the condenser can be estimated from conservation of energy: $Q_{lh} = \alpha \eta q_{solar} A_{leaf}$, where α is the solar absorptivity of the evaporating interface. Crudely approximating

 $\alpha \approx 1$ for our graphite-coated leaf, an average vapor-to-liquid conversion efficiency of $\eta=0.72$, an irradiance of approximately $q_{\rm solar}\approx 0.36$ suns (360 W/m²), and a leaf area of $A_{\rm leaf}=22.9\,{\rm cm}^2$, results in $Q_{\rm lh}\approx 0.6\,{\rm W}$. Of course, the cold plate additionally had a cooling power associated with maintaining its temperature at $T\approx 15\,^{\circ}{\rm C}$ in a room temperature ambient.

The experimental measurements of j_e can be used to estimate the suction generated by a synthetic tree, which equals the sum of viscous losses across the nanoporous disk, viscous losses across the vertical tubes, and the hydrostatic pressure of the liquid columns within the tubes.⁵⁵ Darcy's Law can be used to estimate the viscous pressure drop across the nanoporous disk: $\Delta P_{\rm D} = (Qt)/(\kappa A)$, where Q is the volumetric flow rate, $t = 3.5 \,\mathrm{mm}$ is the thickness of nanopores extending from the top of the tube array to the bottom face of the leaf, A is the cross-sectional area of the disk (diameter 54 mm), and κ is the intrinsic permeability. In turn, $\kappa = (\varphi r_{\text{pore}}^2)/(8\mu\tau)$, for the nanoporous disk, where $\varphi \approx 0.32$ is the porosity, $r_{\rm pore} \approx 80\,{\rm nm}$ is the average pore radius, $\tau \approx 3.5$ is the tortuosity, and μ is the water's viscosity. The Poiseuille equation can be used to estimate the viscous pressure drop across the tubes: $\Delta P_{\rm P} = (8QH\mu)/(\pi NR^4)$, where H = 6 cm is the height of the tubes, $R = 1.59 \,\mathrm{mm}$ is the tube radius, and N is the number of the tubes in parallel. Finally, the hydrostatic pressure drop is simply $\Delta P_{\rm G} = \rho g H$.

In addition to the three positive pressure drops across the tree, a negative Laplace pressure is generated from the concave menisci within the nanoporous leaf

$$P_{\rm L} = -\frac{2\gamma\cos\theta}{r_{\rm pore}},\tag{1}$$

where γ is the surface tension of the water-air interfaces and θ is the contact angle; each meniscus makes with the side walls of its pore. This Laplace pressure is used to overcome the total pressure drop across the tree

$$|P_{\rm L}| = \Delta P_{\rm total} = \Delta P_{\rm D} + \Delta P_{\rm P} + \Delta P_{\rm G}.$$
 (2)

For mass to be conserved, the evaporation mass flow rate from a synthetic tree must equal the liquid mass flow rate up the tree. Therefore, the experimental measurement of $\dot{m}_{\rm e}$ can be used to define the liquid volumetric flow rate across the tree as $Q=\dot{m}_{\rm e}/\rho$. Plugging the proper value for Q into the Darcy and Poiseuille equations, we solve Eq. (2) for $P_{\rm L}$.

Figure 4 graphs the individual pressures drops as well as the magnitude of the Laplace pressure ($|P_{\rm L}| = \Delta P_{\rm total}$), for both the uncoated and coated trees. For either tree, the average Darcy pressure drop was an order of magnitude larger than the hydrostatic pressure drop across the tubes, which in turn was six orders of magnitude larger than the viscous pressure drops across the tubes. The calculated suction pressure to overcome these pressure drops was $P_{\rm L} \approx -4.41\,{\rm kPa}$ for the plain tree and $P_{\rm L} \approx -5.02\,{\rm kPa}$ for the coated tree.

These values can be non-dimensionalized by $P_{\rm L}^* = P_{\rm L}/P_{\rm L,max}$, where $P_{\rm L,max} \approx -1.82$ MPa is the maximum possible Laplace pressure corresponding to $\theta \approx 0^\circ$ in Eq. (1). The non-dimensional pressures were only $P_{\rm L}^* \approx 0.0024$ for the uncoated tree and $P_{\rm L}^* \approx 0.0028$ for the coated tree. This indicates that the transpiration rate is firmly in the evaporation-limited regime, as opposed to a pressure-limited flow. ⁵⁵ In other words, dramatically higher transpiration rates are possible by

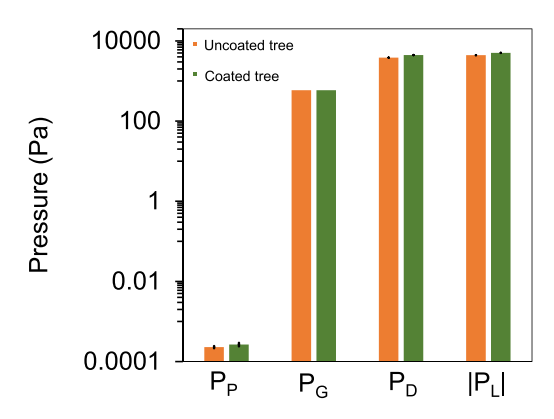


FIG. 4. Calculated absolute values of the negative Laplace pressure in the uncoated and coated trees, found as the sum of the three positive pressure drops. Values shown represent logarithmic plots of the average values, with the error bars corresponding to one standard deviation.

increasing the heat input into the leaf, without running the risk of dryout. Another implication of the low value of $P_{\rm L}^*$ is that, if desired, the tube height H connecting the water reservoir to the evaporating interface could be increased by orders of magnitude if desired.

The transpiration limit for any tree geometry corresponds to the critical mass flow rate, $\dot{m}_{\rm max}$, where the maximum sustainable Laplace pressure ($P_{\rm L,max}$) is required to satisfy Eq. (2). An expression for $\dot{m}_{\rm max}$ is obtained by combining Eqs. (1) and (2), plugging in the expressions for $\Delta P_{\rm D}$, $\Delta P_{\rm P}$, and $\Delta P_{\rm G}$, and substituting $Q = \dot{m}/\rho$,

$$\dot{m}_{\text{max}} = \rho \left(\frac{2\gamma \cos \theta}{r_{\text{pore}}} - \rho g H \right) \left(\frac{t}{\kappa A} + \frac{8H\mu}{\pi N R^4} \right)^{-1}.$$
 (3)

Plugging in all of the aforementioned values to the variables and assuming $\theta \approx 0^{\circ}$, we obtain $\dot{m}_{\rm max} = 9.78 \times 10^{-5}$ kg/s for our current tree geometry. Experimentally, our coated tree exhibited an average evaporation (i.e., transpiration) rate of $\dot{m} = 2.38 \times 10^{-7}$ kg/s, only 0.24% of the maximum possible transpiration rate. The transpiration limit can also be conceptualized as a maximum tree height for a given transpiration rate

$$H_{\text{max}} = \left(\frac{2\gamma \cos \theta}{r_{\text{pore}}} - \frac{\dot{m}t}{\rho \kappa A}\right) \left(\frac{8\dot{m}\mu}{\pi \rho N R^4} + \rho g\right)^{-1}.$$
 (4)

Even when assuming an aggressive transpiration rate of $\dot{m} = 10^{-5} \, \text{kg/s}$ (nearly two orders of magnitude higher than our experimental rate), we obtain a maximum tree height of $H_{\text{max}} \approx 167 \, \text{m}$.

In contrast, the maximum thickness of a conventional solar steam generator, comprised of a floating porous structure, is constrained by the capillary limit. An expression for $t_{\rm max}$ can be estimated by balancing the Laplace pressure against the Darcy pressure

$$t_{\text{max}} = \left(\frac{2\gamma \cos \theta}{r_{\text{pore}}}\right) \left(\frac{\rho \kappa A}{\dot{m}}\right). \tag{5}$$

For a hypothetical scenario of a floating porous structure exhibiting the same pore radius and permeability as the nanopores of our synthetic leaf, we obtain $t_{\rm max} \approx 3.4\,{\rm cm}$ for the same transpiration rate

of $\dot{m}=10^{-5}$ kg/s. The ratio of the maximum height of the evaporating interface for a synthetic tree vs a bulk porous structure is, therefore, an astounding $H_{\rm max}/t_{\rm max}\sim 4866$. This validates that our transpiration-based approach to evaporation can pump the water against gravity to dramatic heights, making it attractive for underground water extraction or perhaps even for pumped storage hydropower.

In summary, we placed a transpiration-powered synthetic tree within a solar still to enhance solar steam generation and water harvesting. Replacing capillary action with transpiration enabled a three-dimensional solar steam generator that thermally decoupled the evaporating surface from the bulk reservoir while also bypassing the capillary limit. A synthetic tree, comprised of a thermally absorptive nanoporous leaf connected to insulating vertical tubing, was shown to harvest three times more water compared to a bulk reservoir. While other solar steam generators have demonstrated a similar enhancement in evaporating and re-condensing water, the height of these systems was constrained to only a few centimeters due to the capillary limit. In contrast, here the rehydration of the evaporating interface is provided by transpiration up millimetric tube conduits, enabling a height rise of many meters if desired. We expect that our tree-based solar steam generator will, therefore, be of interest for applications in underground water extraction and purification. Future research could focus on fabricating taller trees (by having the tubes exit the solar still), utilizing multiple synthetic leaves to increase the area over which evaporation occurs, or incorporating desalination membranes at the tube inlets to prevent salt buildup within the tree when using ocean water.

This work was supported by the National Science Foundation CAREER Award (No. CBET-1653631).

DATA AVAILABILITY

The data that support the findings of this study are available from the corresponding author upon reasonable request.

REFERENCES

¹M. M. Mekonnen and A. Y. Hoekstra, "Four billion people facing severe water scarcity," Sci. Adv. 2, e1500323 (2016).

²H. Ghasemi, G. Ni, A. M. Marconnet, J. Loomis, S. Yerci, N. Miljkovic, and G. Chen, "Solar steam generation by heat localization," Nat. Commun 5, 4449 (2014)

3L. Zhang, B. Tang, J. Wu, R. Li, and P. Wang, "Hydrophobic light-to-heat conversion membranes with self-healing ability for interfacial solar heating," Adv. Mater 27, 4889–4894 (2015).

⁴C. Chang, C. Yang, Y. Liu, P. Tao, C. Song, W. Shang, J. Wu, and T. Deng, "Efficient solar-thermal energy harvest driven by interfacial plasmonic heating-assisted evaporation," ACS Appl. Mater. Interfaces 8, 23412–23418 (2016).

⁵Z. Yu, C. Li, L. Li, J. Yang, and S. Cheng, "Highly efficient solar vapor generator enabled by 3D hierarchical structure constructed with hydrophilic carbon felt for desalination and wastewater treatment," ACS Appl. Mater. Interfaces 11, 32038–32045 (2019).

⁶L. Wu, Z. Dong, Z. Cai, T. Ganapathy, N. X. Fang, C. Li, C. Yu, Y. Zhang, and Y. Song, "Highly efficient three-dimensional solar evaporator for high salinity desalination by localized crystallization," Nat. Commun 11, 521 (2020).

⁷Y. Ito, Y. Tanabe, J. Han, T. Fujita, K. Tanigaki, and M. Chen, "Multifunctional porous graphene for high-efficiency steam generation by heat localization," Adv. Mater. 27, 4302–4307 (2015).

⁸Y. Liu, S. Yu, R. Feng, A. Bernard, Y. Liu, Y. Zhang, H. Duan, W. Shang, P. Tao, C. Song, and T. A. Deng, "Bioinspired, reusable, paper-based system for high-performance large-scale evaporation," Adv. Mater. 27, 2768–2774 (2015).

- ⁹Y. Liu, J. Chen, D. Guo, M. Cao, and L. Jiang, "Floatable, self-cleaning, and carbon-black-based superhydrophobic gauze for the solar evaporation enhancement at the air-water interface," ACS Appl. Mater. Interfaces 7, 13645–13652 (2015).
- ¹⁰J. Lou, Y. Liu, Z. Wang, D. Zhao, C. Song, J. Wu, N. Dasgupta, W. Zhang, D. Zhang, P. Tao, W. Shang, and T. Deng, "Bioinspired multifunctional paper-based RGO composites for solar-driven clean water generation," ACS Appl. Mater. Interfaces 8, 14628–14636 (2016).
- ¹¹Q. Jiang, L. Tian, K. K. Liu, S. Tadepalli, R. Raliya, P. Biswas, R. R. Naik, and S. Singamaneni, "Bilayered biofoam for highly efficient solar steam generation," Adv. Mater. 28, 9400–9407 (2016).
- ¹²C. Liu, J. Hsiung, Y. Tian, J. Wang, Y. Han, and A. Fratalocchi, "High performance large-scale solar steam generation with nanolayers of reusable biomimetic nanoparticles," Adv. Sustainable Syst. 1, 1600013 (2017).
- ¹³H. Zhang, L. Li, B. Jiang, Q. Zhang, J. Ma, D. Tang, and Y. Song, "Highly thermally insulated and superhydrophilic corn straw for efficient solar vapor generation," ACS Appl. Mater. Interfaces 12, 16503–16511 (2020).
- ¹⁴K. Bae, G. Kang, S. K. Cho, W. Park, K. Kim, and W. J. Padilla, "Flexible thinfilm black gold membranes with ultrabroadband plasmonic nanofocusing for efficient solar vapour generation," Nat. Commun 6, 10103 (2015).
- ¹⁵M. Jiang, Q. Shen, J. Zhang, S. An, S. Ma, P. Tao, C. Song, B. Fu, J. Wang, T. Deng, and W. Shang, "Bioinspired temperature regulation in interfacial evaporation," Adv. Funct. Mater. 30, 1910481 (2020).
- ¹⁶T. Li, H. Liu, X. Zhao, G. Chen, J. Dai, G. Pastel, C. Jia, C. Chen, E. Hitz, D. Siddhartha, R. Yang, and L. Hu, "Scalable and highly efficient mesoporous wood-based solar steam generation device: Localized heat, rapid water transport," Adv. Funct. Mater. 28, 1707134 (2018).
- 17 L. Zhou, Y. Tan, D. Ji, B. Zhu, P. Zhang, J. Xu, Q. Gan, Z. Yu, and J. Zhu, "Self-assembly of highly efficient, broadband plasmonic absorbers for solar steam generation," Sci. Adv. 2, e1501227 (2016).
 18 S. Han, J. Yang, X. Li, W. Li, X. Zhang, N. Koratka, and Z. Yu, "Flame synthesis
- ¹⁸S. Han, J. Yang, X. Li, W. Li, X. Zhang, N. Koratka, and Z. Yu, "Flame synthesis of superhydrophilic carbon nanotubes/Ni-foam decorated with Fe₂O₃ nanoparticles for water purification via solar steam generation," ACS Appl. Mater. Interfaces 12, 13229–13238 (2020).
- ¹⁹X. Wu, G. Y. Chen, W. Zhang, X. Liu, and H. Xu, "A plant-transpiration-process-inspired strategy for highly efficient solar evaporation," Adv. Sustainable Syst. 12, 1700046 (2017).
- ²⁰Y. Zhang, S. K. Ravi, and S. C. Tan, "Systematic study of the effects of system geometry and ambient conditions on solar steam generation for evaporation optimization," Adv. Sunstainable Syst. 3, 1900044 (2019).
- ²¹K. Liu, Q. Jiang, S. Tadepalli, R. Raliya, P. Biswas, R. R. Naik, and S. Singamaneni, "Wood-graphene oxide composite for highly efficient solar steam generation and desalination," ACS Appl. Mater. Interfaces 9, 7675–7681 (2017).
- ²²F. Liu, L. Wang, R. Bradley, B. Zhao, and W. Wu, "Graphene-carbon composites for solar and low-voltage powered efficient interfacial evaporation," Adv. Sustainable Syst. 4, 1900122 (2020).
- ²³C. Tian, J. Liu, R. Ruan, X. Tian, X. Lai, L. Xing, Y. Su, W. Huang, Y. Cao, and J. Tu, "Sandwich photothermal membrane with confined hierarchical carbon cells enabling high-efficiency solar steam generation," Small 16, 2000573 (2020).
- ²⁴K. Go, K. Bae, H. Y. Kim, H. Choi, and K. J. Lee, "Solar-to-steam generation via porous black membranes with tailored pore structures," ACS Appl. Mater. Interfaces 11, 48300–48308 (2019).
- ²⁵J. Li, X. Zhou, P. Mu, F. Wang, H. Sun, Z. Zhu, J. Zhang, W. Li, and A. Li, "Ultralight biomass porous foam with aligned heirarchical channels as salt resistant solar steam generators," ACS Appl. Mater. Interfaces 12, 798–806 (2020).
- ²⁶J. He, Z. Zhang, C. Xiao, F. Liu, H. Sun, Z. Zhu, W. Liang, and A. Li, "High-performance salt-rejecting and cost-effective superhydrophilic porous monolithic polymer foam for solar steam generation," ACS Appl. Mater. Interfaces 12, 16308–16318 (2020).
- ²⁷D. Zhao, H. Duan, S. Yu, Y. Zhang, J. He, X. Quan, P. Tao, W. Shang, J. Wu, C. Song, and T. Deng, "Enhancing localized evaporation through separated light absorbing centers and scattering centers," Sci. Rep. 5, 17276 (2015).

- ²⁸Y. Zhang, S. K. Ravi, L. Yang, J. V. Vaghasiya, L. Suresh, I. Tan, and S. C. Tan, "Portable trilayer photothermal sructure for hybrid energy harvesting and synergic water purification," ACS Appl. Mater. Interfaces 11, 38674–38682 (2019).
- ²⁹Z. Li, C. Wang, T. Lei, H. Ma, J. Su, S. Ling, and W. Wang, "Arched bamboo charcoal as interfacial solar steam generation integrative device with enhanced water purification capacity," Adv. Sustainable Syst. 3, 1800144 (2019).
- 30Y. Wang, H. Liu, C. Chen, Y. Kuang, J. Song, H. Xie, C. Jia, S. Kronthal, X. Xu, S. He, and L. Hu, "All natural, high efficient groundwater extractionvia solar steam/vapor generation," Adv. Sustainable Syst. 3, 1800055 (2019).
- ³¹C. Wang, Y. Wang, X. Song, M. Huang, and H. Jiang, "A facile and general strategy to deposit polypyrrole on various substrates for efficient solar-driven evaporation," Adv. Sustainable Syst. 3, 1800108 (2019).
- ³²N. Xu, X. Hu, W. Xu, X. Li, L. Zhou, S. Zhu, and J. Zhu, "Mushrooms as efficient solar steam-generation devices," Adv. Mater. 29, 1606762 (2017).
- 33M. Zhu et al., "Tree-inspired design for high-efficiency water extraction," Adv. Mater. 29, 1704107 (2017).
- ³⁴Z. Liu, B. Wu, B. Zhu, Z. Chen, M. Zhu, and X. Liu, "Continuously producing watersteam and concentrated brine from seawater by hanging photothermal fabrics under sunlight," Adv. Funct. Mater. 29, 1905485 (2019).
- 35G. W. Koch, S. C. Sillett, G. M. Jennings, and S. D. Davis, "The limits to tree height," Nature 428, 851–854 (2004).
- ³⁶A. D. Stroock, V. V. Pagay, M. A. Zwieniecki, and N. M. Holbrook, "The physicochemical hydrodynamics of vascular plants," Annu. Rev. Fluid Mech. 46, 615–642 (2014).
- ³⁷N. M. Holbrook and M. A. Zwieniecki, Vascular Transport in Plants (Academic Press, 2011).
- ³⁸P. F. Scholander, "How mangroves desalinate seawater," Physiol. Plant 21, 251–261 (1968).
- ³⁹A. K. Parida and B. Jha, "Salt tolerance mechanisms in mangroves: A review," Trees 24, 199–217 (2010).
- ⁴⁰K. Kim, E. Seo, S. K. Chang, T. J. Park, and S. Lee, "J. Novel water filtration of saline water in the outermost layer of mangrove roots," Sci. Rep. 6, 20426 (2016).
- ⁴¹I. Paudel, A. Naor, Y. Gal, and S. Cohen, "Simulating nectarine tree transpiration and dynamic water storage from responses of leaf conductance to light and sap flow to stem water potential and vapor pressure deficit," Tree Physiol. 35, 425–438 (2015).
- ⁴²T. D. Wheeler and A. D. Stroock, "The transpiration of water at negative pressures in a synthetic tree," Nature 455, 208–212 (2008).
- 43T. D. Wheeler and A. D. Stroock, "Stability limit of liquid water in metastable equilibrium with subsaturated vapors," Langmuir 25, 7609–7622 (2009).
- 44 J. Li, C. Liu, Z. Xu, K. Zhang, X. Ke, and L. Wang, "A microfluidic pump/valve inspired by xylem embolism and transpiration in plants," PLoS One 7(11), e50320 (2012).
- ⁴⁵O. Vincent, P. Marmottant, P. A. Quinto-Su, and C. D. Ohl, "Birth and growth of cavitation bubbles within water under tension confined in a simple synthetic tree," Phys. Rev. Lett 108, 184502 (2012).
- 46C. Duan, R. Karnik, M. C. Lu, and A. Majumdar, "Evaporation-induced cavitation in nanofluidic channels," Proc. Natl. Acad. Sci. U.S.A 109, 3688–3693 (2012).
- ⁴⁷O. Vincent, D. A. Sessoms, E. J. Huber, J. Guioth, and A. D. Stroock, "Drying by cavitation and poroelastic relaxations in porous media with macroscopic pores connected by nanoscale throats," Phys. Rev. Lett 113, 134501 (2014).
- ⁴⁸M. Lamb, G. W. Koch, E. R. Morgan, and M. W. Shafer, "A synthetic leaf: The biomimetic potential of graphene oxide," Proc. SPIE **9429**, 942915–942910 (2015).
- ⁴⁹I. T. Chen, D. A. Sessoms, Z. Sherman, E. Choi, O. Vincent, and A. D. Stroock, "Stability limit of water by metastable vapor-liquid equilibrium with nanoporous silicon membranes," J. Phys. Chem. B 120, 5209–5222 (2016).
- 50]. M. Li, C. Liu, Z. Xu, K. P. Zhang, X. Ke, C. Y. Li, and L. D. Wang, "A bio-inspired micropump based on stomatal transpiration in plants," Lab Chip 11, 2785–2789 (2011).

- ⁵¹J. Comtet, K. H. Jensen, R. Turgeon, A. D. Stroock, and A. E. Hosoi, "Passive phloem loading and long-distance transport in a synthetic tree-on-a-chip," Nat. Plants 3, 1–8 (2017).
- ⁵²M. Lee, H. Lim, and J. Lee, "Fabrication of artificial leaf to develop fluid pump driven by surface tension and evaporation," Sci. Rep. 7, 14735 (2017).
- ⁵³C. Finnerty, L. Zhang, D. L. Sedlak, K. L. Nelson, and B. Mi, "Synthetic graphene oxide leaf for solar desalination with zero liquid discharge," Environ. Sci. Technol. 51, 11701–11709 (2017).
- 54Z. Lu, K. L. Wilke, D. J. Preston, I. Kinefuchi, E. Chang-Davidson, and E. N. Wang, "An ultrathin nanoporous membrane evaporator," Nano Lett 17, 6217–6220 (2017).
- 55W. Shi, R. Dalrymple, C. McKenny, D. Morrow, Z. Rashed, D. Surinach, and J. Boreyko, "Passive water ascent in a tall, scalable synthetic tree," Sci. Rep 10, 230 (2020).
- ⁵⁶B. Mi, C. Finnerty, and K. Conway, "Prospects of artificial tree for solar desalination," Science 25, 18–25 (2019).
- 57Y. Wang, J. Lee, J. Weber, and M. Elimelech, "Capillary-driven desalination in a synthetic mangrove," Sci. Adv. 6, eaax5253 (2020).
- ⁵⁸O. L. Hansen, A. B. Sheen, K. M. Swedberg, K. W. Vitale, S. M. Wray, M. D. Fox, and J. B. Boreyko, "Thermally absorptive blankets for highly efficient snowbank melting," Langmuir 34, 2606–2609 (2018).